

The performance of activated carbon in Al-ion based supercapacitors

B. Shenbagabalakrishnan*, V. Gayathri

Nanomaterials Research Laboratory, Department of Physics, Thiagarajar College of Engineering, Madurai - 625015, India

Received: February 07, 2023; Revised: May 09, 2023

Activated carbon (AC), an extraordinary material, is vital in supercapacitor applications. The use of flower stalks from coconut tree (FSCT), as a raw material for synthesis is the highlight of our research. AC is produced by utilizing aluminium chloride hexahydrate ($\text{AlCl}_3 \cdot 6\text{H}_2\text{O}$) as an activating agent in the chemical activation procedure. The BET surface area of the synthesized carbon material is about $50 \text{ m}^2\text{g}^{-1}$ with high content of micropores. In this context, most of the pores have a 0.5-1 nm diameter. AC demonstrates excellent electrochemical performance in 5M aqueous aluminium nitrate nonahydrate ($\text{Al}(\text{NO}_3)_3 \cdot 9\text{H}_2\text{O}$) electrolyte and exhibits a specific capacitance value of 64 Fg^{-1} at 0.1 Ag^{-1} and equivalent serial resistance (ESR) of 23Ω , measured by impedance spectroscopy. It is worth noting that the retention of the capacitance of the electrode was sufficiently high even after 1000 cycles.

Keywords: Flower stalks, Amorphous carbon, Activating agent, Al ion, Supercapacitor, Capacitance retention, Nyquist plot

INTRODUCTION

Clean, renewable energy production and energy storage is the primary solution to environmental pollution and the depreciation of fossil fuels [1]. The requirements of high energy and power density are the main scope of research in energy and fuels [2]. Various techniques are available to improve the supercapacitors energy density, e.g., the presently investigated hybrid capacitors, composite electrodes and multivalent ion-based electrolytes [3]. Multivalent ion-based electrolytes got great attention compared to univalent ion electrolytes due to the larger number of electron transitions [4]. Aluminium is an excellent multivalent ion electrolyte among others, due to its smaller ionic radius, high volumetric and gravimetric capacity and safety aspects [5]. Since the size of an electrolyte ion is smaller than the size of a micropore of AC, it can access a larger specific surface area of the pores, which leads to achieving an increased value of specific capacitance [6]. In this context, the Al ion with low ionic radius is a more suitable electrolyte ion for porous electrodes to enhance the specific capacitance. Carbon is a pearl in the sea of energy storage due to its properties such as inertness and stability of material with a wide potential window, cost-effectiveness and abundance [7]. Porous carbon, among other forms of carbon structures, is well adopted in energy storage, CO_2 capture, hydrogen storage and water treatment applications [8-10]. Hence, it becomes a promising electrode material.

Physical and chemical activation are the two techniques adopted to obtain activated carbon [11, 12]. The second route is the simplest and most efficient way of getting AC using chemical agents like KOH and ZnCl_2 [13-15]. Compared to other activating routes, KOH-based

activation has produced highly microporous AC [16]. In recent times, the performances of AC as an electrode in different electrolytes are highlighted in the literature as follows: $\text{H}_4\text{P}_2\text{O}_7$ -activated carbon from leather waste has a surface area of $381 \text{ m}^2\text{g}^{-1}$, which gives a specific capacitance of 550 Fg^{-1} in 6M KOH electrolyte [17].

Biomass is activated by KOH pre-treatment for 18 h. It has a high micropore surface area of $639 \text{ m}^2\text{g}^{-1}$ and a pore volume of $0.26 \text{ cm}^3\text{g}^{-1}$, which gives a specific capacitance of 162 Fg^{-1} in 6M KOH electrolyte [18]. Spent coffee grounds precursor is activated with KOH at a ratio of 1:1.5, affording a specific surface area of $2330 \text{ m}^2\text{g}^{-1}$, providing a specific capacitance of 84 F/g^{-1} at 1 A g^{-1} in 1M Na_2SO_4 electrolyte [19]. Some authors have used H_3PO_4 as an activating agent to prepare durian shell-based AC with a surface area of $2004 \text{ m}^2\text{g}^{-1}$ and a pore diameter of 3.34 nm. They have reported a specific capacitance of 93.1 Fg^{-1} in 1.5M Na_2SO_4 electrolyte [20].

Novel activated carbon will be produced by an original chemical activation procedure, using aluminium chloride as an activating agent. The micropores of activated carbon play an important role in enhancing the specific capacitance of the supercapacitor. It is worth mentioning that AlCl_3 is expected to improve the porosity of the carbon. To our knowledge, there are no literature data on the production of activated carbon with this activating agent.

EXPERIMENTAL

The flower stalks of the coconut tree (FSCT) were taken as the source of carbon, and aluminium chloride hexahydrate ($\text{AlCl}_3 \cdot 6\text{H}_2\text{O}$ [A.R. grade from Kempasol, India]) was used as an activating agent. Aluminium nitrate nonahydrate ($\text{Al}(\text{NO}_3)_3 \cdot 9 \text{H}_2\text{O}$) from Merck acted as an aqueous electrolyte. The raw fresh FSCT was thoroughly

* To whom all correspondence should be sent:
E-mail: bshenbagabalakrishnan@gmail.com

washed with distilled water to remove dirt and impurities, followed by a complete sundry. Then it was heated for 6 h in a muffle furnace at 500° C. The activating agent was prepared by mixing AlCl₃ powder with distilled water at 0.1 mg/ml concentration. Carbon powder of weight 0.5 g already derived from flower stalks was soaked in this solution for 24 h and then rinsed several times with distilled water to remove any residuals present in the material. After this step, it was completely dried out for hours and then heated in a microwave oven for 3 min. Thus, we get the microporous carbon which is ready to use. The methodology of our work is presented in Fig. 1. The structural analysis of the sample was performed using Bruker D8 Advance X-ray diffractometer, with Cu K α as the source and scintillation counter as a detector. The measured angle ranged from 10° to 80°, as shown in Fig. 2(a). To investigate the disorders and the presence of impurities, Raman spectra of the sample were recorded with a He–Cd laser of 325 nm wavelength (Horiba Jobin Yvon of LabRAM HR Evolution Model). The Raman spectrum for the sample was taken in the range of 0 to 4000 cm⁻¹, which is indicated in Fig. 2(b). The morphological studies of the sample were performed on a VEGA3 TESCAN scanning electron microscope. The SEM image in the 2 μ m range with a magnification of 10kX is shown in Fig. 3(a). Jeol / JEM 2100 HRTEM with

LaB6 electron gun was used to study the surface nature of the sample, and the images in the 20 nm scale are presented in Fig. 3(b). BET surface area and pore analysis were performed with the help of BELSorp – max, BEL Japan, Inc. For this, the degassing temperature was fixed at 200°C at a pressure of 2.096 \times 10⁻⁴ Pascal and kept for 2 h to remove the adsorbed impurities on the sample, if any.

The ‘as-prepared’ AC was investigated to evaluate its electrochemical properties with the help of an Auto lab electrochemical workstation. Further analysis was carried out by cyclic voltammetry (CV), Galvan static charge/discharge (GCD) and EIS. All the data were taken through a standard three-electrode system. For this study, platinum wire was taken as a counter electrode, Ag/AgCl as a reference electrode and a 3 mm diameter glassy carbon as a working electrode. The sample was pasted on the bottom of the surface, which is a working electrode in a mass of 1.12 mg and dried at 70°C for 12 h. The sample consisted of 80% active material (AC), 15% carbon black, and 5% PTFE as a binder. To get better results, the working electrode was dipped into 5M aqueous Al-ion electrolyte (prepared from Al(NO₃)₃ powder) for 2 h before starting the measurement. The CV studies were recorded in the potential range from 0 to 1 V, and the EIS analysis was carried out by applying input frequency in the range of 10 kHz to 0.1 Hz at a perturbation of 5 mV.

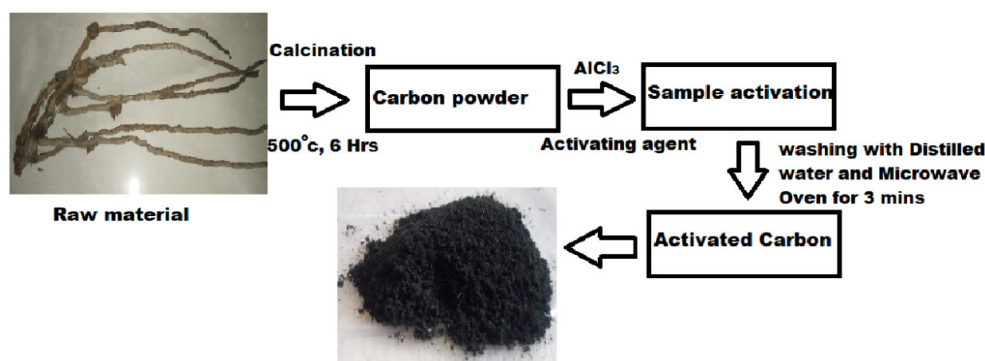


Figure 1. Step-by-step preparation process of AC from FSCT

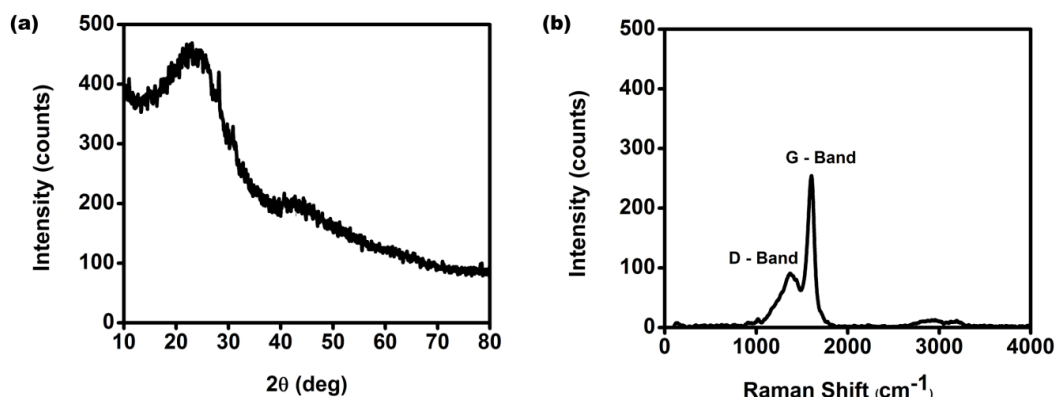


Figure 2. (a) XRD pattern of AC prepared from flower stalks of the coconut tree; (b) Raman spectrum of the AC sample showing the peaks of D and G-bands

RESULTS AND DISCUSSION

X-ray diffraction analysis

The prepared AC sample was probed through X-ray diffraction analysis. The following information was then congregated. The prominent peaks' positions in 2θ angle were around 25° and 44° shown in Fig. 2(a), which represent (002) and (100) planes of orientation, respectively (compared with JCPDS No: 75-1621) [21]. At the same time, the broad width of the peak shows that it is an amorphous material; that is, its crystallite size is very small (i.e., ~ 1 nm). This concise range of definite orderly atom arrangements also confirms its amorphous nature [22]. There are two conflict peaks observed in the Raman spectrum corresponding to D-band (1369 cm^{-1}) and G-band (1604 cm^{-1}), which are presented in Fig. 2(b). In addition, the spectrum also shows a broad peak with lower intensity in and around 3000 cm^{-1} , which we predict to come from the 2D band. In the Raman spectra, the vibration from the C=C in-plane is called a G-band. This deliberately indicates the purity of carbon materials [23], whereas the D-band comes from the 'out of plane vibrations'. This evinces the structural disorder like vacancies or adsorbed impurities that befall. The intensity of the D-band dropped when contrasted with the G-band, i.e., the I_D / I_G ratio (0.36) substantiated that the level of defects is very low [24].

Scanning electron microscopy analysis

The SEM image illustrates the sheet-like morphology of the sample, which is shown in Fig. 3(a), whereas the

HRTEM seems spongy and permeable in nature, as presented in Fig. 3(b) and also exhibits a larger number of narrow pores on the surface. The pore diameter measured from the TEM image is approximately in the range of 2 to 10 nm. The obtained data demonstrate that the nitrogen low-temperature adsorption isotherm (Fig. 4(a)) belongs to type-I according to IUPAC classification, where the amount of adsorbed nitrogen gas molecules approaches saturation of total pore volume at a limiting value of $17\text{ cm}^3\text{g}^{-1}$. This uptake is governed by the accessible micropore volume rather than the internal surface area. A steep uptake at very low p/p_0 is due to enhanced adsorbent-adsorptive interactions in narrow micropores, resulting in micropore filling. Generally, for nitrogen and argon adsorption at 77K and 87K, microporous materials of width $< \sim 1\text{ nm}$ give type-I(a) isotherms whereas materials having pore size distributions over a broader range, including wider micropores and possibly narrow mesopores ($< \sim 2.5\text{ nm}$), show type-I (b) isotherms. Our sample having micro and mesopores exhibits a type-I(b) isotherm, as expected. The obtained results indicated an H4 hysteresis loop that agrees with the IUPAC classification for a sample with micro-mesoporous nature [25]. This was further confirmed by Barrett, Joyner, and Halenda's (BJH) plot, where we observed the diameter of most of the pores to be $\sim 0.9\text{ nm}$, occupying almost 90% of the sample volume. Pores of diameter ranging from 0.4 nm to 2 nm were also present in this sample within a smaller volume, as presented in Fig. 4(b). The sample's surface area was calculated through BET, and it worked out to be $50\text{ m}^2\text{g}^{-1}$.

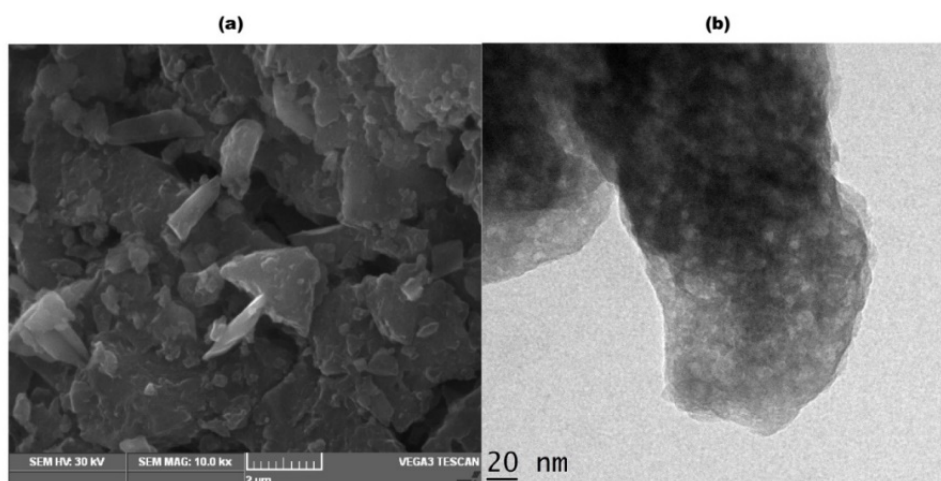


Figure 3. (a) SEM image of AC; (b) as-prepared AC HRTEM image with magnification

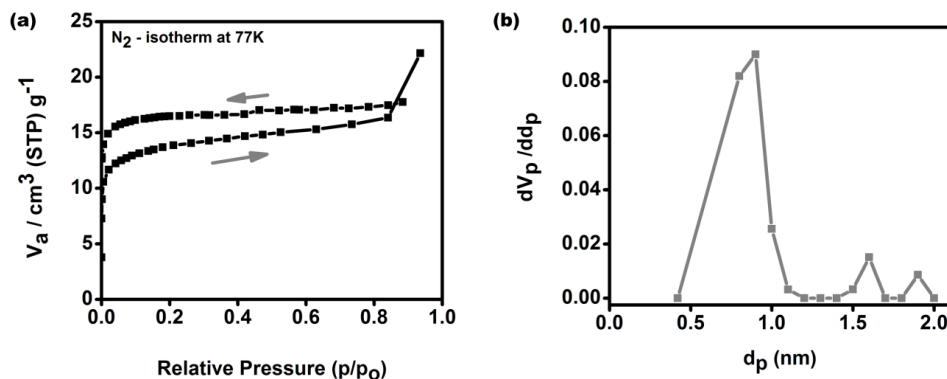


Figure 4. (a) N_2 adsorption and desorption isotherm; (b) pore size distributions of AC

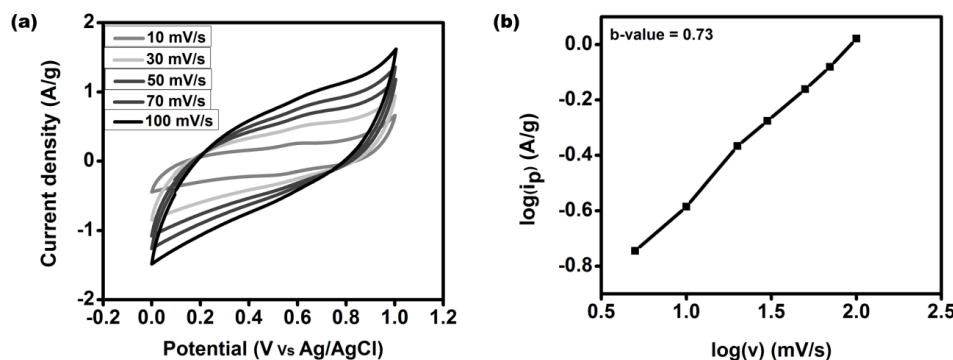


Figure 5. (a) CV of AC at various scan rates ranging from 10 mVs^{-1} to 100 mVs^{-1} ; (b) b-value graph for the AC electrode plotted in-between scan rate and peak current of cathodic sweeps

Electrochemical behavior

To understand the electrochemical behavior of the sample, a three-electrode system was employed in the CV and GCD measurements. The CV was measured over the sample's potential range of 0 to 1V in 5 M $\text{Al}(\text{NO}_3)_3$ electrolytic solutions. The CV showed that the sample exhibits a quasi-rectangular shape because of the double layer and pseudo-capacitance behavior, as shown in Fig. 5(a). The pseudo-capacitance behavior was due to the intercalation/deintercalation of Al ions into the pores of AC [30]. The contribution of pseudo capacitance was high at the lower scan rate, and became less when the scan rate was increased while at the lower scan rate, the ions get enough time to intercalate into the pores of AC [31].

There occurred a cathodic peak at 0.6V and an anodic peak at 0.5V. Therefore, if no peak occurs, the EDLC's contribution significantly affects the higher scan rate [26]. Fig. 5(b) shows that the cathodic peak current linearly varies according to the corresponding scan rates. In this context, the calculated b-value of 0.73 confirms the presence of dual capacitance. From Fig. 6(a), let's compare the galvanostatic charge and discharge profiles of two different current densities with individual time scales. The tiger-tooth-shaped charge and discharge patterns deliberately show the existence of dual capacitance. This is discussed briefly in the CV curve itself. In particular, around 30% of its total charge was given while discharging, and the remaining charges were delivered slowly. The short time taken for charging and discharging depicts its high suitability for supercapacitor

applications. The specific capacitance calculated from GCD at 0.1 Ag^{-1} was 64 Fg^{-1} and was compared with other electrolytes, (see Table 1). From this, we can see that our sample provides high specific capacitance even at the low surface area for dual capacitance. Further, the feature of micropores of the AC and low ionic radius of the Al^{3+} ions also contribute to this enhancement.

Fig. 6(b) gives the exponential variation of the specific capacitance concerning the current density. The capacitance retention rate for 1000 cycles was gradually amplified due to the electrochemical activation of the electrode through the diffusion of Al^{3+} ions into the pores consecutively during GCD, as given in Fig. 6 (c). This is confirmed by the enlargement of the CV curve taken after the GCD cycles compared to the starting state, as shown in Fig. 7(a). Fig. 7 (b) shows the sample's complex plane plot (Nyquist plot). It unveils the impedance in different frequency regions. We have obtained an ESR value of $\sim 23 \Omega$, corresponding to the kinetics of Al^{3+} ions on the surface of the electrode. The absence of semi-circle reveals that the activated carbon manifests EDLC nature [28], and the slope at just above 45° angle in the low-frequency region elucidates the diffusion limitations due to the intercalation/deintercalation of Al^{3+} ions into the pores [29]. After several cycles, the impedance spectrum slightly reduces the ESR value. Also, the angle of slope deviates from capacitor's behavior and confirms the electrode's electrochemical activation through the diffusion of Al^{3+} ions into the pores, as indicated in Fig. 7 (b).

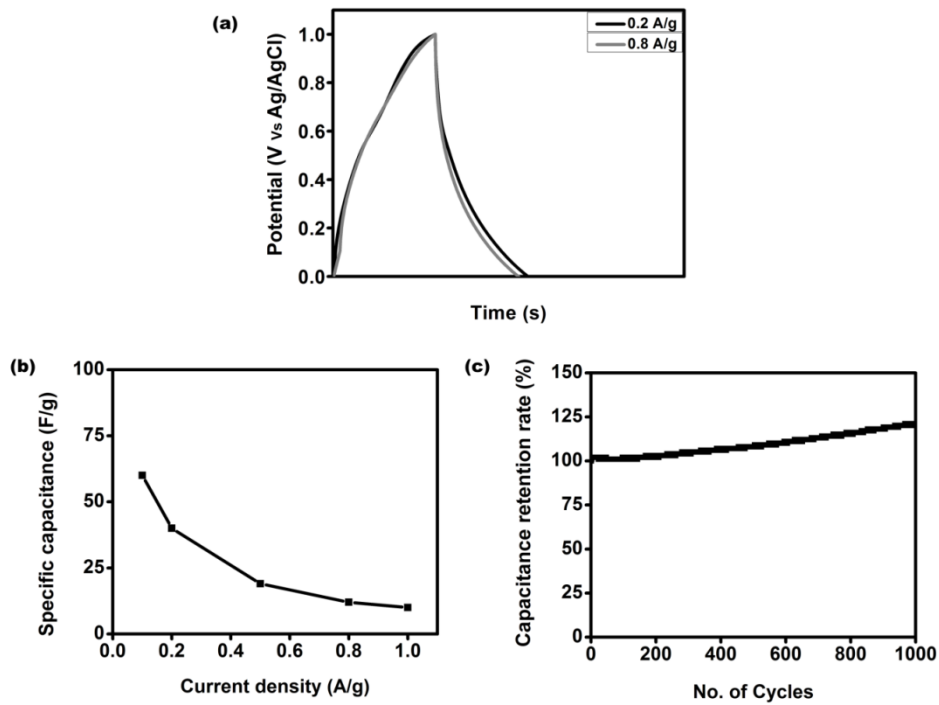


Figure 6. Comparison of the GCD curve for two different current densities: (a) 0.2 and 0.8 Ag^{-1} ; (b) calculation of specific capacitance for AC electrode for various current densities from 0.1 to 1 Ag^{-1} ; (c) retention of specific capacitance up to 1000 GCD cycles.

Table 1. Performance of AC with different electrolytes

Electrolyte	Surface area (m^2g^{-1})	Avg. pore diameter (nm)	Specific capacitance (Fg^{-1})	Potential window (V)	Ref.
1M Na_2SO_4	2330	-	84	1.9	[19]
1M H_2SO_4	614	3.4	74	0.8	[30]
6M KOH	900	2.32	73	0.9	[31]
5M $\text{Al}(\text{NO}_3)_3$	50	0.9	64	1	This work

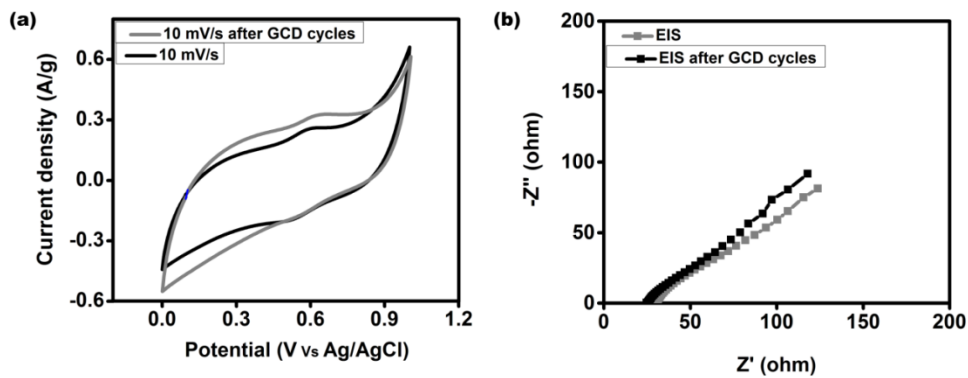


Figure 7. Cyclic voltammograms and complex plane plots of AC before (a) and after (b) 1000 GCD cycles.

CONCLUSIONS

In the present work, we have incorporated two novel ideas: an electrolyte based on multivalent ions and an electrode of AC prepared using $\text{AlCl}_3 \cdot 6\text{H}_2\text{O}$ as an activating agent. AC prepared from flower stalks from the coconut tree (natural and inexpensive) proved to be an efficient electrode material with outstanding performance as a supercapacitor with Al ion-based electrolyte. The prepared sample has amorphous nature with very slight structural defects. The as-prepared AC exhibited double-layer capacitance, as well as pseudo-capacitance behavior. This dual behavior is due to the intercalation/deintercalation of Al ions into the pores of the AC. This becomes one of the most important factors in giving a high specific capacitance value of 64 Fg^{-1} , even though the sample's surface area is low. From this analysis we concluded that AlCl_3 can also effectively act as an activating agent to create micropores on the surface of AC. Further, enlargement of the surface area is possible by increasing the ratio between the activation agent and carbon, which is in progress. We could observe that this nature-derived AC is aptly suitable for aqueous-based Al ion supercapacitor applications.

Conflicts of interest: The authors declare no conflicts of interest.

REFERENCES

1. G. Olabi, C. Onumaegbu, T. Wilberforce, M. Ramadan, M. A. Abdelkareem, A. H. Al-Alami, *Energy*, **214**, 118987 (2021).
2. K. Sharma, A. Arora, S. K. Tripathi, *J. Energy Storage*, **21**, (2019).
3. J. Cao, H. Xu, J. Zhong, X. Li, S. Li, Y. Wang, M. Zhang, H. Deng, Y. Wang, C. Cui, M. Hossain, Y. Cheng, L. Fan, L. Wang, T. Wang, J. Zhu, B. Lu, *ACS Appl. Mater. Interface*, **13**, 7 (2021).
4. Ponrouch, J. Bitenc, R. Dominko, N. Lindahl, P. Johansson, M. R. Palacin, *Energy Storage Mater.*, **20**, 253 (2019).
5. S. K. Das, S. Mahapatra, H. Lahan, *J. Mater. Chem. A*, **5** (14), 6347 (2017).
6. J. A. Lin Ritter, B. N. Popov, *J. Electrochem. Soc.*, **146** (10), 3639 (1999). Y. Wang, L. Zhang, H. Hou, W. Xu, G. Duan, S. He, K. Liu, S. Jiang, *J. Mater. Sci.*, **56**(1), 173 (2020).
7. M. Mohan, V. K. Sharma, E. A. Kumar, V. Gayathri, *J. Energy Storage*, **1** (2), 35 (2019).
8. S. He, G. Chen, H. Xiao, G. Shi, C. Ruan, Y. Ma, H. Dai, B. Yuan, X. Chen, X. Yang, *J. Colloid Interface Sci.*, **582**, 90 (2021).
9. S. A. Borghei, M. H. Zare, M. Ahmadi, M. H. Sadeghi, A. Marjani, S. Shirazian, M. Ghadiri, *Arab. J. Chem.*, **14** (2), 102958 (2021).
10. H. Shang, Y. Lu, F. Zhao, C. Chao, B. Zhang, H. Zhang, *RSC Adv.*, **5** (92), 75728 (2015).
11. M. Sevilla, R. Mokaya, *Energy Environ. Sci.*, **7** (4), 1250 (2014).
12. M. M. Baig, I. H. Gul, *Biomass and Bioenergy*, **144**, 105909 (2021).
13. S. Suhdi, C. Wang, *Appl. Sci.*, **11** (9), 3994 (2021).
14. Z. Higai, E. Huang, W. Qian, *Environ. Prog. Sustain. Energy*, **40** (2) (2020).
15. R. Hidayu, N. Muda, *Procedia Eng.*, **148**, 06 (2016).
16. S. I. El-Hout, S. Y. Attia, S. G. Mohamed, S. M. Abdelbasir, *J. Environ. Manag.*, **304**, 114222 (2022).
17. G. A. Yakaboyle, C. Jiang, T. Yumak, J. W. Zondlo, J. Wang, E. M. Sabolsky, *Renew. Energy*, **163**, 276 (2021).
18. L. Adan-Mas, P. Alcaraz, F. Arévalo-Cid, A. López-Gómez, F. Montemor, *J. Waste Manag.*, **120**, 280 (2021).
19. J. P. Tey, M. A. Careem, M. A. Yarmo, A. K. Arof, *Ionics*, **22** (7), 1209 (2016).
20. P. Mavin, J. Wirat, L. Paveena, *Mater. Res. Express*, **9**, 065603 (2022).
21. B. R. Puri, L. R. Sharma, *ShobanLalNagin Chand and Co*, **313** (1992).
22. S. Divya T. Nann, *ChemElectroChem*, **8** (3), 492 (2020).
23. R. D. Nagarajan, A. K. Sundramoorthy, *Sens. Actuators B Chem.*, **301**, 127132 (2019).
24. M. Thommes, *Chem. Int.*, **38** (1), 25 (2016).
25. K. C. Tsay, L. Zhang, J. Zhang, *Electrochim. Acta*, **60**, 428 (2012).
26. X. Luo, Y. Chen, Y. Mo, *New Carbon Mater.*, **36**, 49 (2021).
27. B. E. Conway, *Electrochemical supercapacitors: scientific fundamentals and technological applications*. Springer Science & Business Media, 2013.
28. M. A. Scibioh, B. Viswanathan, *Materials for Supercapacitor Applications*, Elsevier, 2020, p. 336.
29. M. Jain, M. Ghosh, S. Krajewski, Kurungot, M. Michalska, *J. Energy Storage*, **34**, 102178 (2021).
30. M. P. Chavhan, S. Ganguly, *Ionics*, **23**, 2037 (2017).